An in-depth spectroscopic examination of molecular bands from 3D hydrodynamical model atmospheres

A. Gallagher, E. Caffau, P. Bonifacio, H.-G. Ludwig, M. Steffen, D. Homeier, B. Plez

HAL Id: hal-01862777
https://hal.umontpellier.fr/hal-01862777

Submitted on 16 Jan 2021

Astronomy & Astrophysics

LETTER TO THE EDITOR

An in-depth spectroscopic examination of molecular bands from 3D hydrodynamical model atmospheres

II. Carbon-enhanced metal-poor 3D model atmospheres

A. J. Gallagher[1,*], E. Caffau[1], P. Bonifacio[1], H.-G. Ludwig[2,1], M. Steffen[3,1], D. Homeier[2], and B. Plez[4]

[1] GEPI, Observatoire de Paris, PSL Research University, CNRS, Université Paris Diderot, Sorbonne Paris Cité, place Jules Janssen, 92190 Meudon, France
e-mail: andrew.gallagher@obspm.fr
[2] Zentrum für Astrononmie der Universität Heidelberg, Landessternwarte, Königstuhl 12, 69117 Heidelberg, Germany
[3] Leibniz-Institut für Astrophysik Potsdam, An der Sternwarte 16, 14482 Potsdam, Germany
[4] Laboratoire Univers et Particules de Montpellier, LUPM, Université de Montpellier, CNRS, 34095 Montpellier Cedex 5, France

ABSTRACT

Context. Tighter constraints on metal-poor stars we observe are needed to better understand the chemical processes of the early Universe. Computing a stellar spectrum in 3D allows one to model complex stellar behaviours, which cannot be replicated in 1D.
Aims. We examine the effect that the intrinsic CNO abundances have on a 3D model structure and the resulting 3D spectrum synthesis.
Methods. Model atmospheres were computed in 3D for three distinct CNO chemical compositions using the CO^{5}BOLD model atmosphere code, and their internal structures were examined. Synthetic spectra were computed from these models using Linfor3D and they were compared. New 3D abundance corrections for the *G*-band and a selection of UV OH lines were also computed.
Results. The varying CNO abundances change the metal content of the 3D models. This had an effect on the model structure and the resulting synthesis. However, it was found that the C/O ratio had a larger effect than the overall metal content of a model.
Conclusions. Our results suggest that varying the C/O ratio has a substantial impact on the internal structure of the 3D model, even in the hot turn-off star models explored here. This suggests that bespoke 3D models, for specific CNO abundances should be sought. Such effects are not seen in 1D at these temperature regimes.

Key words. hydrodynamics – radiative transfer – line: formation – molecular processes – stars: chemically peculiar

1. Introduction

Carbon-enhanced metal-poor (CEMP) stars are a class of metal-poor star that exhibit overabundances in carbon, relative to their iron abundance; [C/Fe] > +1.0 (Beers & Christlieb 2005). To date, CEMP stars represent roughly 1/5th of the known population of metal-poor stars (Lucatello et al. 2006). They can be further categorised according to their neutron-capture element abundances, giving rise to four subclasses: CEMP-no, CEMP-r/s, CEMP-r, and CEMP-s. Formal definitions of these subclasses are given in Beers & Christlieb (2005). Spite et al. (2013) found that when the absolute carbon abundances, *A*(C), of CEMP stars are presented as a function of [Fe/H], two distinct bands are found; the high and low carbon bands. This work was subsequently extended in Bonifacio et al. (2015). The high carbon band contains the most iron-rich CEMP stars, and is populated by all four subclasses of CEMP star. Evidence suggests that most, if not all of these stars attained their high *A*(C) through possible binary interaction; typically, these stars show radial velocity variations that are indicative of a faint companion (Lucatello et al. 2005). None of the stars on the low carbon band demonstrate an overabundance in the heavy elements, although the available upper limits on [Ba/Fe] are not precise enough to allow a firm classification as CEMP-no stars. It would

appear that these stars formed from gas clouds that were previously enriched with carbon. However, the process(es) by which these gas clouds procured their enhanced *A*(C) is still highly debated (see Salvadori et al. 2015, and references therein). Therefore, tighter constraints from observations are highly sought so that the chemical processes in the early Universe can be better understood. This in turn requires the use of more sophisticated modelling of the stellar atmosphere to compute more realistic synthetic spectra.

In the first paper in this series, (Gallagher et al. 2016a, henceforth Paper I), we recently published a grid of 3D *A*(C) corrections for several dwarf star models. They were computed by fitting 1D synthetic *G*-band profiles to 3D *G*-band profiles, essentially treating the 3D synthetic profiles as observed data of known *A*(C). These syntheses were computed using the temperature structures of 3D model atmospheres that have normal metal-poor chemical compositions, and the CNO abundances were then enhanced for the spectrum synthesis. This presented clear inconsistencies between the intrinsic chemical composition of the model and the chemical composition of the synthetic spectra.

It is common practice to assume that the iron abundance of a star, [Fe/H], is equal to its metal content, so that $\log Z/Z_\odot \approx$ [Fe/H]. A simple calculation shows that while an [Fe/H] = −3.0 metal-poor star with [α/Fe] = +0.4 has a metal content by mass

Table 1. Model and syntheses abundances used in the present investigation.

Model ID	Model abundances				Model Δt (s)	Synthesis ID	Syntheses abundances				Comment
	A(C)	A(N)	A(O)	C/O			A(C)	A(N)	A(O)	C/O	
A	5.39	4.78	6.06	0.21	50600	**SAB**	7.39	6.78	6.06	21.4	Inconsistent
						SAC	7.39	6.78	7.66	0.54	Inconsistent
B	7.39	6.78	6.06	21.4	45200	**SB**	7.39	6.78	6.06	21.4	Consistent
C	7.39	6.78	7.66	0.54	71600	**SC**	7.39	6.78	7.66	0.54	Consistent

Notes. All models were computed using identical stellar parameters $T_{\rm eff}$/$\log g$/[Fe/H] = 6250 K/4.0/−3.0. Abundances of syntheses **SAB** and **SAC** computed using model **A** were artificially enhanced to match the intrinsic abundances of models **B** and **C**, making them inconsistent with the intrinsic CNO abundances of model **A**. This is how 3D corrections were computed in Paper I. "Model Δt" refers to difference in time (in seconds) between the first and last snapshot selected in the model series.

fraction of $Z \approx 2.75 \times 10^{-5}$ (or $\log Z/Z_\odot \approx -2.71$), a CEMP star with ΔA(CNO) = +2 dex, with the same [Fe/H], has a $Z \approx 1.66 \times 10^{-3}$ ($\log Z/Z_\odot \approx -0.93$), which is almost two orders of magnitude larger. It was already demonstrated in Paper I that the 3D temperature gradient (as a function of $\log \tau_{\rm ROSS}$) of a metal-poor model is steeper than a more metal-rich model, and that molecular formation is heavily influenced ultimately by the temperature structure of the model. Molecular opacities in turn influence the temperature structure of the model. Therefore, it could be argued that the 3D metal-poor models utilised in Paper I were not appropriate to compute G-band spectra of CEMP stars. We present a significant test that examines whether intrinsic 3D CEMP models are necessary for modelling molecular spectral features in stars with peculiar CNO abundances. We also assess this supposition by computing new 3D corrections for the synthetic G-band using these new models and compare them to corrections computed from spectra synthesised using a metal-poor model. It has been shown that CNO abundances only matter in 1D at lower temperatures (Plez & Cohen 2005; Gustafsson et al. 2008; Masseron 2008).

2. Model atmospheres and spectrum synthesis

The work presented here required the computation of 3D model atmospheres. They were computed with CO⁵BOLD (Freytag et al. 2012) using the box-in-a-star mode. All models were computed with identical stellar parameters $T_{\rm eff}$/$\log g$/[Fe/H] = 6250 K/4.0/−3.0, but the model chemical composition was varied. Our investigation also called for the computation of 3D synthetic spectra. As the features of interest were molecular bands, we computed them with Linfor3D[1], which was recently modified to compute large spectral regions (Gallagher et al. 2016b).

Appendix A presents a brief investigation under 1D, which is analogous to the one detailed here.

2.1. CO⁵BOLD model computations

The CO⁵BOLD 3D model atmospheres consist of a series of 20 computational boxes, referred to as snapshots. The snapshots were selected from a larger temporal sequence of computational boxes that have reached full dynamical and thermal relaxation. The snapshots selected are spaced far enough apart in time (∼58 characteristic timescales[2]) to be considered statistically

independent. The spatial resolution and geometrical size of all atmospheres were $140 \times 140 \times 150$ grid points representing a $26.1 \times 26.1 \times 12.8$ Mm region of the stellar atmosphere. Opacities were based on OSMARCS model opacities (these models are used in Appendix A), which were binned into 14 opacity groups (Nordlund 1982; Ludwig et al. 1994). The effect of scattering was treated according to the Hayek et al. (2010) approximation as explored by Collet et al. (2011); scattering opacities in the deeper layers of the model are treated as true absorption and ignored in the outer regions of the model atmosphere (see Ludwig & Steffen 2013, for a full description). As all models used are metal poor, the alpha elements were enhanced so that [α/Fe] = +0.4. A summary of the models computed for this investigation, and their intrinsic CNO abundances, are presented in Table 1. The nomenclature given in this table is used throughout this work for clarity. The opacity sources for each model include the effects associated with changing A(CNO) (e.g. CH, OH, C, etc.). We did not account for changes in the thermodynamic properties of the plasma due to the enhancement of the CNO abundances, and used the same equation-of-state table for all three models. While the change of the relative number of metallic atoms is indeed substantial (increasing from 2×10^{-6} to 7×10^{-5}), the overall number fraction remains minute. As such, we do not expect a noticeable impact on molecular weight, specific heat, etc. of the plasma, which are mostly controlled by hydrogen and helium.

Each 3D model atmosphere has two counterpart model atmospheres, which are computed for the same stellar parameters and model chemical composition. The first is an external 1D model atmosphere computed using the Lagrangian HydroDynamics (LHD) model atmosphere code (Caffau & Ludwig 2007). LHD model atmospheres use the same microphysics approximations (equation-of-state, opacities, etc.) adopted by the 3D models. The second is an averaged, ⟨3D⟩, model atmosphere computed for each 3D snapshot by spatially averaging the thermal structure of the computational box over surfaces of equal Rosseland optical depth.

2.2. Spectrum synthesis

Synthetic spectra for the CH G-band (4140−4400 Å) and the CN BX-band (3870−3890 Å) features, as well as 14 UV OH transitions (3122−3128 Å), which we refer to as the OH-band, were computed for this analysis. The line list used to synthesise the G-band is described in Paper I. The line list used for the CN-band was identical to that detailed in Gallagher et al. (2016b). The line list of the OH-band was adopted from part of the OH line list used by Spite et al. (2017).
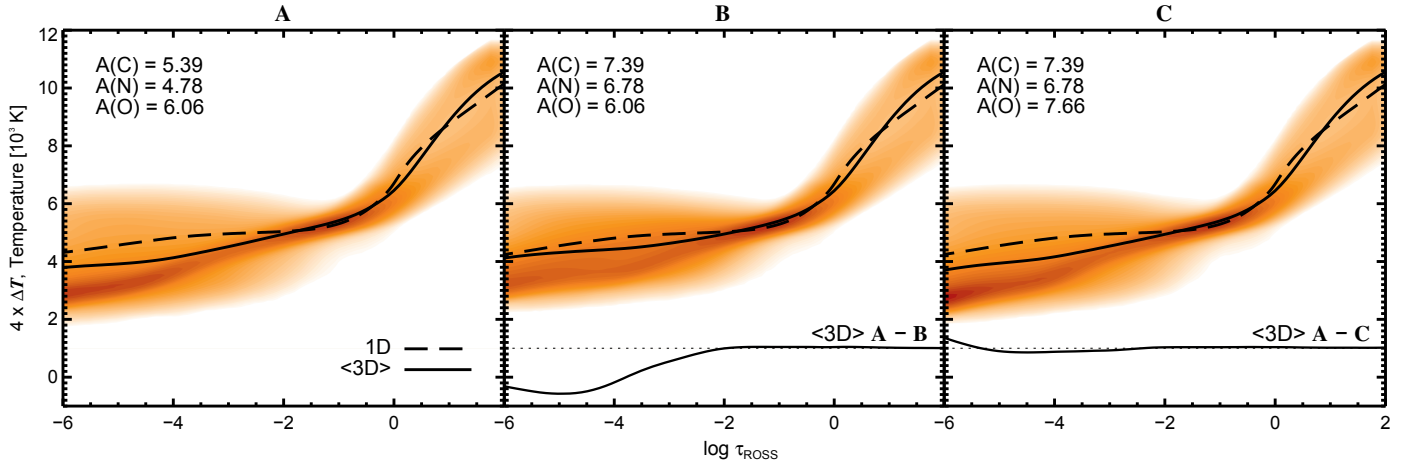
---

[1] http://www.aip.de/Members/msteffen/linfor3d
[2] $t_{\rm c} = H_{\rm P}/c$, where $H_{\rm P}$ and c are the pressure scale height at $\log \tau_{\rm ROSS}$ = 1 and sound speed, respectively.

Fig. 1. Temperature structures of the three model atmospheres analysed in this investigation. The intrinsic CNO abundances are given in each panel. Details about each model and the synthesis produced with them is given in Table 1. Panels **B** and **C** also present the differences between the $\langle 3D \rangle$ temperature structures of model **A** with models **B** and **C** respectively. This has been scaled up four times relative to the y-axis to better show the temperature deviations so that every tick represents a $\Delta T = 50$ K.

The chemical compositions input into Linfor3D for the syntheses of the two CEMP model atmospheres, **B** and **C**, were were identical to the models' intrinsic chemical structures. As such, a single *G*-band, CN-band, and OH-band spectrum was computed for each of these models, which we refer to as **SB** and **SC**. The chemical abundances used to compute syntheses from model **A** were enhanced to match the chemical compositions of models **B** and **C**, resulting in the synthesis of two *G*-band, CN-band and OH-band spectra, called **SAB** and **SAC**, see Table 1.

Every 3D synthetic spectrum had two counterpart spectra, which were computed using the 1D LHD and $\langle 3D \rangle$ model atmospheres. The spectra from these two models are computed along with the 3D spectra in Linfor3D to help distinguish the effects that the stellar granulation (3D to $\langle 3D \rangle$) and the lower average temperatures ($\langle 3D \rangle$ to 1D) in the outermost regions have on the resultant spectra.

3. Results

Figure 1 depicts the temperature structures of models **A**, **B** and **C** and presents how the chemical composition affects the thermal structure of the 3D models, and their counterpart 1D LHD and $\langle 3D \rangle$ model atmospheres. For clarity, we also present the $\langle 3D \rangle$ temperature differences between model **A** and models **B** and **C** in the centre and right panels of the figure. The temperature differences of the 1D models are not presented as they are almost identical. It is clear that changes to the chemical composition of a model do impact the 3D temperature stratification. The C/O[3] ratio of models **A** and **B** differ the most. If they are compared, the temperature fluctuations become smaller in **B**, and the average temperature, $\langle 3D \rangle$, increases by up to 400 K in the outermost regions of the atmospheres. However, when models **A** and **C** are compared, the mean temperature and temperature fluctuations are very well reproduced. This suggests that the C/O ratio is more important to the model structure than the overall metal content, *Z*. This indicates that when the C/O ratio is high, the blanketing effect of carbon-bearing molecules other than CO affect the temperature structure of the 3D model, which in turn would also affect the absorbing strength of the CH- and CN-bands.

---

[3] $X/Y = N(X)/N(Y) = 10^{[A(X)_* - A(Y)_*]}$. The $A(C) - A(O)$ ratio can also be considered instead.

Table 2. 3D abundance corrections, $\Delta_{3D} = A(C)_{3D} - A(C)_{1D,LHD}$, for the *G*-band and the OH-band from the models examined in this work.

Model ID	Synthesis ID	Δ_{3D}	
		G-band	OH-band
A	**SAB**	-0.76	-0.40
	SAC	-0.31	-0.88
B	**SB**	-0.50	-0.35
C	**SC**	-0.32	-0.73

Figure 2 depicts the equivalent width contribution functions of the *G*-band, CN-band, and OH-band. This function is derived by integrating the line-depth contribution function (Magain 1986) over all wavelength points sampled during the spectrum synthesis. An equivalent width contribution function is useful as its integral reproduces the equivalent width of the feature, allowing us to compare the contribution of the various atmospheric layers to the total absorption that makes up a spectral feature. The black lines represent the contribution functions of the spectra **SB** (top) and **SC** (bottom), while the red lines are those from **SAB** (top) and **SAC** (bottom). The formations of the **SB** and **SAB** (i.e. C/O = 21.4) CN- and *G*-bands are drastically different, while the formations of **SC** and **SAC** (i.e. C/O = 0.54) are fairly comparable. As was explained in Paper I, the oxygen- and carbon-bearing molecules – more specifically CH and OH – have an anti-correlated interrelationship. The difference in behaviour between **SC** and **SAC** in the OH-band is not as significant as is seen in **SB** and **SAB** for the CH *G*-band. The scenario presented here only alters the C/O ratio by changing $A(O)$ while $A(C)$ is fixed. Appendix A in Paper I demonstrated that when $A(O)$ is fixed and the carbon is allowed to vary, the formation of OH behaves very much like CH, although in an anti-correlated manner.

Table 2 provides 3D corrections, $\Delta_{3D} = A(C)_{3D} - A(C)_{1D,LHD}$, of the *G*-band and OH-band. Based on the behaviours of **SC** and **SAC** for the *G*-band in Fig. 2, and the corrections of **SB** and **SAB** in Table 2, the 3D corrections to the *G*-band presented in Paper I are still valid, as the C/O ratio used for those syntheses (0.21) is comparable to **SAC** and **SC** (0.54). When the C/O ratio is large (case **SB** and **SAB**), the 3D corrections are no longer similar and the large correction provided by **SAB** is reduced by 0.26 dex by
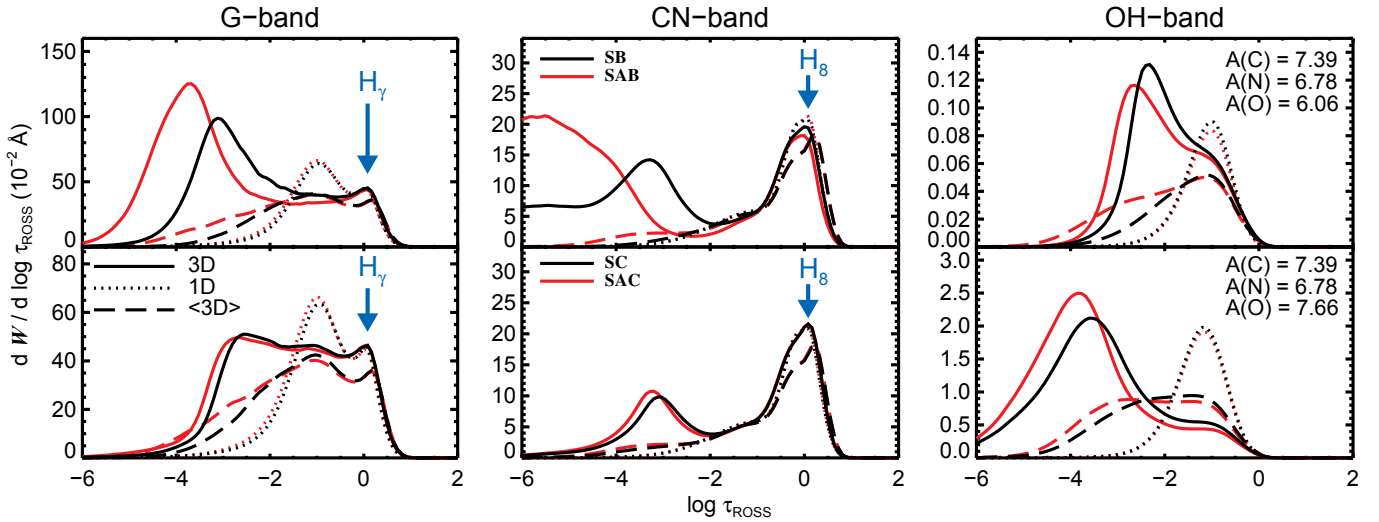
Fig. 2. 3D, ⟨3D⟩, and 1D contribution functions of the *G*-, CN- and OH-bands. *Top*: comparison between **SB** and **SAB**. *Bottom*: comparison between **SC** and **SAC**. Indicators have been marked in the *G*-band and CN-band to show where the Balmer features are forming in these bands.

SB. This also supports the previous work performed on the C/O ratio in Paper I. The corrections provided by the OH-band further demonstrate the anti-correlated behaviour with CH. When the C/O ratio is small, the excess oxygen not used to form CO, forms more OH. The opposite is seen for the *G*-band. It was decided that it would be inappropriate to include *A*(N) corrections from a comparative analysis of the *G*-band and CN-band because we have not investigated the additional impact *A*(N) will have on this band or the model atmospheres, and also because of the extreme behaviour seen in the CN-band formation; the CN-band forms outside the confines of the computational box in syntheses **SB** and **SAB**.

4. Discussion and conclusions

We have confirmed that a large, non-solar-like C/O ratio affects the structure of a 3D model (models **A** and **B**, Fig. 1). We have also shown that this impacts the synthetic spectra computed from them (syntheses **SB** and **SAB**, Fig. 2). The cooler average temperature of model **A** relative to **B** allows for the formation of higher number densities of CH and CN in shallower regions of the atmosphere when **SAB** is synthesised assuming LTE. The higher temperatures of model **B** reduces overall line strength of **SB** and partially restricts molecule formation in the outer regions, pushing formation inward (see the *G*- and CN-bands for syntheses **SB** and **SAB**, Fig. 2). In this regime, the 3D corrections from **SAB** are overestimated and should be replaced by the consistent corrections from **SB**. Figure 2 also demonstrates that, in contrast to 3D, inconsistencies in the chemical composition of the 1D LHD models do not impact the synthetic 1D spectra, as they do not probe the temperature ranges where these models form in large quantities. This means that errors do not cancel in the 3D-1D differential approach because the inconsistencies in the intrinsic chemical composition matter for 3D, but not for 1D.

We have demonstrated in a limited fashion that the overall effect the CNO abundance has on the 3D model structure is small if the C/O ratio remains fairly consistent between the models and syntheses at this temperature regime, as presented by models **A** and **C** and by syntheses **SC** and **SAC**. In this scenario, model **C** has a C/O ratio that is approximately twice as large as is found in model **A**, as *A*(C) in model **C** is +2.0 dex larger than in model **A**. Nevertheless, synthesis **SAC** appropriately replicates synthesis

SC for both carbon molecular bands. This is supported by the consistent 3D corrections found in **SC** and **SAC** for the *G*-band, given in Table 2. At this point in time, it is not possible to empirically determine the C/O value at which a new model must be computed as the syntheses from a model like **A** will become unreliable. From the models analysed here, it would seem that the impact that *A*(C) has on the thermal structure is minimal as long as C/O < 1, but it becomes significant when C/O > 1.

We have explored the CN-band in detail. As was foreshadowed by Bonifacio et al. (2013) and Gallagher et al. (2016b), the abundances determined from the standard 3D model are unreliable when the C/O > 1.0, as a significant fraction of its formation occurs outside the confines of the computational box. We confirm this behaviour in synthesis **SAB**, and show that it is greatly improved by synthesis **SB** but not fully resolved. In both instances, C/O = 21.4. Interestingly, we can see that this is a purely 3D effect, due to the stellar granulation, as the ⟨3D⟩ and 1D syntheses do not trace the behaviour of the 3D contribution functions lower than $\log \tau_{ROSS} < -2$, and only a very small amount of formation in the region $-5 \le \log \tau_{ROSS} \le -3$ can be attributed to the lower average temperature of model **A** relative to **B** (as shown by the red and black dashed lines in Fig. 2, top middle panel). However, inspection of the granulation patterns of all three models do not reveal any obvious differences in granulation size or behaviour. It has been established that the CN-band is sensitive to departures from thermodynamic equilibrium (NLTE), and it is also known that part of the CN-band forms in the chromosphere of the Sun (Mount & Linsky 1975). Studies by Peterson & Schrijver (1997) and Takeda & Takada-Hidai (2011) both confirm that metal-poor dwarf stars have a chromosphere. Further exploration of the CN-band behaviour in 3D is warranted. The additional effect *A*(N) has on the formation of the CN-band should also be considered.

This work presents a first step into a new area of research in 3D stellar atmosphere modelling. Based on spectroscopic analyses carried out in 1D for decades, it was generally understood that the metal abundance pattern of a model (i.e. anything beyond helium) had little-to-no effect on the metal-poor model as the total mass fraction was imperceptibly changed. Under the 3D caveat, we have found that this is also held, but only when the C/O ratio is roughly consistent between model and synthesis.

When this changes, the model structure changes enough to affect the resulting spectra computed from them. If this is not taken into account, it can lead to line formation outside the computational box, over- or underestimations in the strength of the feature, and inappropriate 3D corrections. We intend to extend this work and provide a detailed analysis for a larger number of 3D CEMP models.

References

Beers, T. C., & Christlieb, N. 2005, ARA&A, 43, 531
Bonifacio, P., Caffau, E., Ludwig, H.-G., et al. 2013, Mem. Soc. Astron. It. Suppl., 24, 138
Bonifacio, P., Caffau, E., Spite, M., et al. 2015, A&A, 579, A28
Caffau, E., & Ludwig, H.-G. 2007, A&A, 467, L11
Collet, R., Hayek, W., Asplund, M., et al. 2011, A&A, 528, A32
Freytag, B., Steffen, M., Ludwig, H.-G., et al. 2012, J. Comput. Phys., 231, 919
Gallagher, A. J., Caffau, E., Bonifacio, P., et al. 2016a, A&A, 593, A48
Gallagher, A. J., Steffen, M., Caffau, E., et al. 2016b, ArXiv e-prints
    [arXiv:1610.04427]
Gustafsson, B., Edvardsson, B., Eriksson, K., et al. 2008, A&A, 486, 951
Hayek, W., Asplund, M., Carlsson, M., et al. 2010, A&A, 517, A49
Kurucz, R. L. 2005, Mem. Soc. Astron. It. Suppl., 8, 14
Lucatello, S., Tsangarides, S., Beers, T. C., et al. 2005, ApJ, 625, 825
Lucatello, S., Beers, T. C., Christlieb, N., et al. 2006, ApJ, 652, L37
Ludwig, H.-G., & Steffen, M. 2013, Mem. Soc. Astron. It. Suppl., 24, 53
Ludwig, H.-G., Jordan, S., & Steffen, M. 1994, A&A, 284, 105
Magain, P. 1986, A&A, 163, 135
Masseron, T. 2008, in First Stars III, eds. B. W. O'Shea, & A. Heger, AIP Conf. Ser., 990, 178
Mount, G. H., & Linsky, J. L. 1975, ApJ, 202, L51
Nordlund, A. 1982, A&A, 107, 1
Peterson, R. C., & Schrijver, C. J. 1997, ApJ, 480, L47
Plez, B., & Cohen, J. G. 2005, A&A, 434, 1117
Salvadori, S., Skúladóttir, Á., & Tolstoy, E. 2015, MNRAS, 454, 1320
Spite, M., Caffau, E., Bonifacio, P., et al. 2013, A&A, 552, A107
Spite, M., Peterson, R. C., Gallagher, A. J., Barbuy, B., & Spite, F. 2017, A&A, in press, DOI: 10.1051/0004-6361/201630058
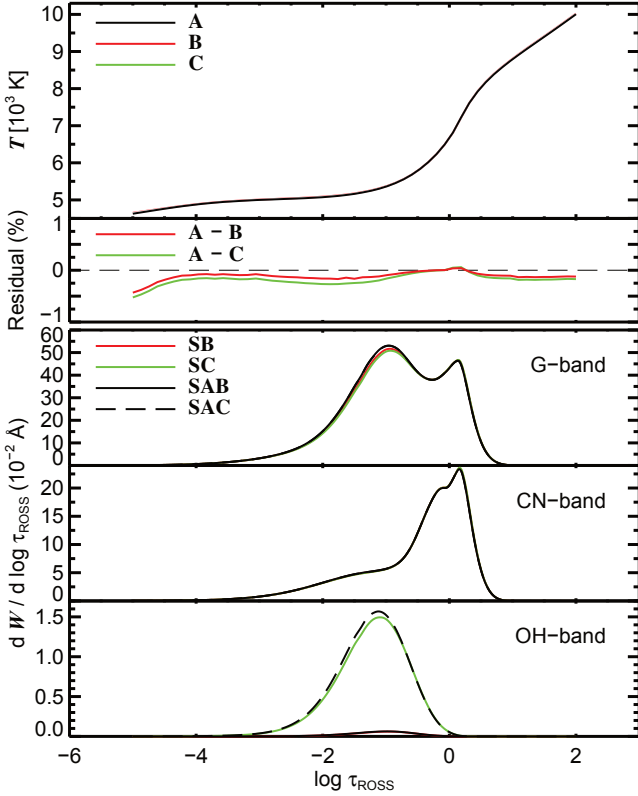Takeda, Y., & Takada-Hidai, M. 2011, PASJ, 63, 547

Fig. A.1. 1D OSMARCS temperature structures for the model abundances given in Table 1 and the residuals (*top two panels*). Resulting contribution functions for the CH- CN- and OH-bands are given in the *bottom three panels*. The contribution functions for the CN-band are indistinguishable.

Fig. A.2. 1D ATLAS12 temperature structures for the model abundances given in Table 1 and the residuals (*top two panels*). Resulting contribution functions for the CH- CN- and OH-bands are given in the *bottom three panels*. The contribution functions for the CN-band are indistinguishable.
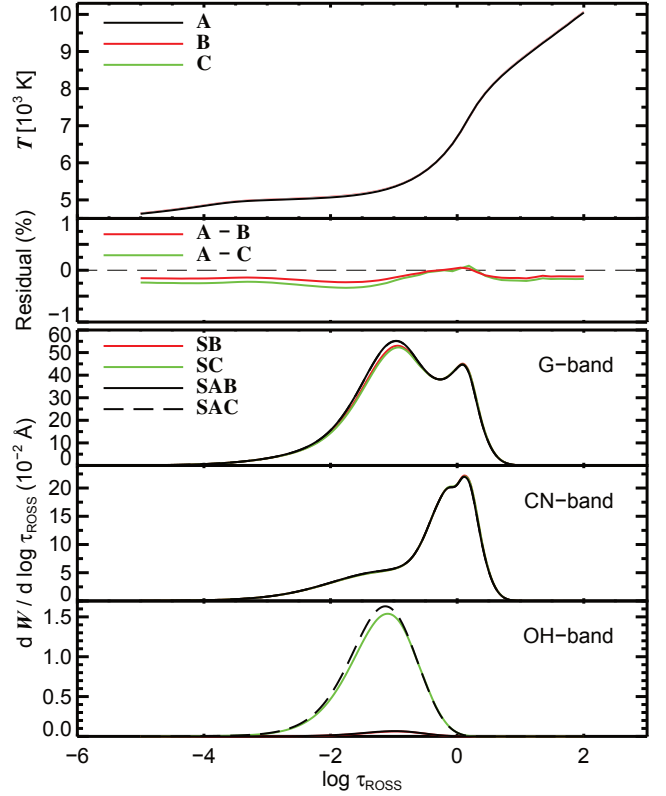
Appendix A: CEMP model atmospheres in 1D

We present the results and conclusions from our 1D investigation, which was carried out to confirm that model chemical abundances have little-to-no effect on the resulting spectrum synthesis for the stellar parameters $T_{\rm eff}/\log g/[{\rm Fe/H}] = 6250\,{\rm K}/4.0/-3.0$. We utilised three 1D OSMARCS (Gustafsson et al. 2008) and three 1D ATLAS12 (Kurucz 2005) model atmospheres. These models have the same three distinct chemical abundances as models **A**, **B** and **C**, given in Table 1. Syntheses were computed in Linfor3D with these models using the same procedures described in Sect. 2.2. As such, we refer to them using the same nomenclature established above.

The temperature structures of the 1D OSMARCS models are presented in Fig. A.1. For better resolution, the relative temperature difference between model **A** with models **B** and **C** is given as a percentage in the second panel. As depicted, the intrinsic chemical structures have a very limited influence on the temperature structure. In fact, it is shown in the second panel that the differences in temperature between **A** and the two CEMP models, **B** and **C**, change the temperature by less than 0.5% towards the outermost layers of the model. Between the regions $-4 \le \log \tau_{\rm ROSS} \le 0$, where lines and continua form in 1D, the changes in the temperatures structures are even smaller.

To test the effect that these minute changes in temperature have on the resulting syntheses, the equivalent width contribution functions of the three molecular bands used in the 3D analysis are also given in Fig. A.1 (bottom three panels). The

change in atmosphere and model chemistry has very little effect on the formation and strength of the carbon bands. As expected, the OH-band behaves differently as the change in $A({\rm O})$ directly changes its formation and strength. However, the differences between **SAB** and **SB** and the differences between **SAC** and **SC** are too small to change $A({\rm O})$ that would be determined by a comparative fit of them.

When we conduct the same tests with the ATLAS12 models (Fig. A.2), we find extremely similar result. In fact, the differences in the temperature structures between **A**, **B**, and **C** are even smaller than were found in Fig. A.1 in the outer most layers of the models. The equivalent width contribution functions from the three molecular bands are also remarkably similar to those computed using the OSMARCS models and the differences between **SAB** and **SB**, and between **SAC** and **SC** are virtually indistinguishable.

The subtle differences found between the ATLAS12 and OSMARCS model structures are too small to significantly influence the resulting spectra computed from them as the largest deviations are found in regions in the model where line formation does not take place. Based on the data presented above, we conclude that the intrinsic chemical structure of a 1D model is unimportant to the resulting syntheses used to model CEMP star spectra, and that artificially enhancing the relevant CNO abundances during the spectral synthesis process is sufficient in the 1D caveat at this temperature regime. This is because CNO opacities have no strong effect on the temperature structure, making it independent of their abundances.